ENVISIONING CONNECTION DETAIL FOR CONNECTING CONCRETE FILLED TUBE (CFT) COLUMNS TO CAP BEAM FOR HIGH SPEED RAIL APPLICATION

Quarterly Progress Report

For the period ending February 29, 2020

Submitted by:

Sheharyar e Rehmat, Research Assistant

Islam Mantawy, Ph.D. Research Assistant Professor

Atorod Azizinamini, Ph.D., P.E., Director, ABC-UTC

Affiliation: Department of Civil and Environmental Engineering
Florida International University
Miami, FL

ACCELERATED BRIDGE CONSTRUCTION
UNIVERSITY TRANSPORTATION CENTER

Submitted to:

ABC-UTC

Florida International University

Miami, FL

1 Background

The demand for mass transit in urban transportation has increased substantially with an increase in the population. Conventional modes of transportation such as road and air travel have caused congestion and traffic problems in many cities around the world. A direct consequence of this is an increase in carbon emissions from automobiles which have contributed to the greenhouse effect. Besides environmental degradation, the cost of road and air travel has been rising with the cost of fuel.

To achieve high mobility for mass transit, there have been innovations in rail transportation. One such example is the introduction of High-speed railway (HSR) which offers a robust alternative to traditional trains, vehicular and air traffic systems for mid-range distances. As technological innovations improve over time, the concept of high speed has also evolved. Since its introduction in 1964, the speed of HSR has increased from 200 Km/hr to about 500 Km/hr. HSR services now operate in more than 16 countries and carry millions of passenger trips per year. It is estimated that a total of 37,000 Km of HSR lines are in operation [Kang, 2018].

HSR offers an efficient, fast and safe transportation system. HSR is one of the best examples of low carbon logistics and offers an additional benefit of lesser greenhouse emissions. Countries with a wide network of high-speed trains have shown a reduction in volumes of road and air traffics. On the other hand, the HSR system is expensive and generally cannot be used for freight transport. The high cost is generally attributed to many factors including dedicated infrastructure, energy requirements, high maintenance etc.

1.1 HSR Systems in Asia and Europe

The introduction of HSR in Europe and Asia in mid-sixties has been a cornerstone in the economic development of many countries. HSR now operate up to 16 countries, and many new countries like Turkey, Saudia Arabia etc are developing HSR systems. Figure 1 shows the percentage of HSR in the world by mileage.

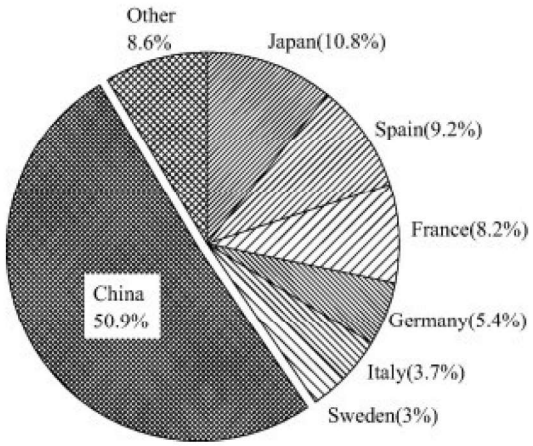

Figure 1. HSR mileage by countries [Hu et. al 204]

Japan was the first country to developed HSR, commonly known as Shinkansen, which operated between Tokyo and Osaka in the sixties. Later on, the Shinkansen network was expanded to different cities covering a total distance of 2800 km. The average speed of these HSR ranges from 260 Km/hr to 320 Km/r. The success of the system relies on dedicated tracks with no level

crossings which has resulted in zero crashes or fatalities since 1964 when these HSR were introduced. Japan is now looking into commercial deployment of Maglev train systems which can achieve up to 550 Km/hr.

China started as late as 2007-2008, and, since then it has developed the largest network of HSR in the world. As of 2016, China has 22,000 Km [Qin, 2017]. The Chinese high-speed train operates at a speed of 350-380 Km/hr. China has also developed Maglev technology which operates on a short route with a maximum speed of 430 Km/hr [Gourvish, 2010]. Figure 2 summarizes different generations of technologies used in different countries.

Europe has an estimated HSR line of almost 6637 Km which are mainly located in France, Germany, Spain, and Italy. Additional high-speed lines are either being constructed or planned for future [Dobruszkes, 2011]. In France, the TGV (Train à Grande Vitesse) was introduced in 1981 between Paris and Lyon. The total network of HSR in France is about 1,800 Km. With technological advancements, the HSR has improved, and, by 2008 the trains achieved the highest operational speed in the world at 320 Km/hr. Spain launched the high-speed train also known as AVE (Alta Velocidad Espanola) in 1992 between the Madrid-Sevilla corridor and now has the largest HSR system in Europe only next to China. Germany developed ICE (Inter City Express) in 1991 which is the long-distance rail transport system. Until 2018, Germany has an HSR network of almost 1658 Km. Other European countries like Turkey, Poland, Switzerland and, Belgium have also developed HSR networks.

Generation	Japan	France	Germany	China
1G	**S-0** 210 km/h 1964 **S-100** 270 km/h 1975 **E-2** 275 km/h 1997	**TGV-PSE** 280 km/h 1981 **TGV-A** 300 km/h 1989	**ICE-1** 250 km/h 1991 **ICE-2** 280 km/h 1996	**CRH1** 200 km/h **CRH2** 200 km/h **CHR5** 200 km/h 2007 **Imported 1G**
2G	**S-500** 300 km/h 1998	**TGV-Mediterranee** 320 km/h **TGV-EST** 2001 320 km/h 2007	**ICE-3** 300 km/h 2002 (Valaro)	**CRH2** 300 km/h **CRH3** 300 km/h 350 km/h **EST** 2008 **Developed 2G**
3G	**Fastech360** 2011 Reduced to 320 km/h, as E5 was put in service	**AGV360** 2008 Tested 360 km/h **EST** in Italy, by 2013 (not over) 300 km/h **EST**	**ICE350E** 2006 Tested 350 km/h **EST** in Spanish (not in service)	**CRH380-A** **CRH380-B** 2010 350-380 km/h In service **Created 3G**

Figure 2. Footmarks of technology development for high-speed trains around the world

1.2 HSR System in United States

The U.S. started its efforts in HSR in the 1960s which resulted in the introduction of Metroliner between New York and Washington D.C. The Federal Railway Administration (FRA) has identified different corridors for connecting populated centers with HSR which are in the range of 100-600 miles. Figure 3 shows different planned corridors. Recent developments include HSR systems planned for California and Texas.

The California High-Speed Rail Authority (CHSRA) envisions a speed of 220 mph with an initial stretch between Los Angeles and San Francisco. The Texas Central Railway and private companies are conducting a study on Dallas to Houston corridor which is almost 250-miles long.

Designated High-Speed Rail Corridors and the North East Corridor

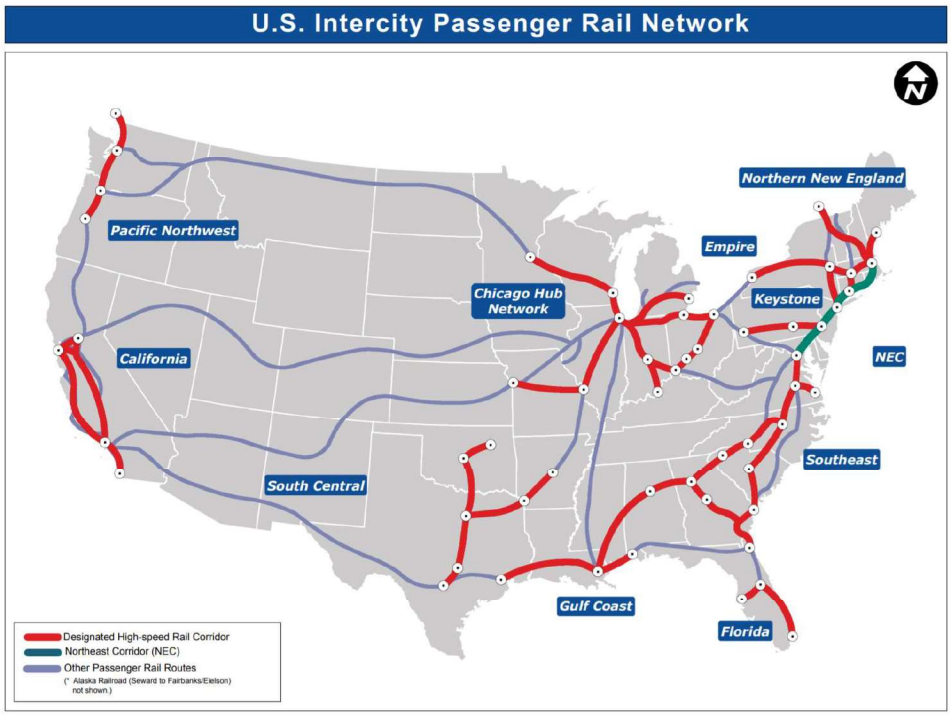

Figure 3. Planned High Speed Rail Corridors in The U.S. [USDOT]

Due to the geography and terrain of California, most of the rail network will use structures which are elevated. The substructure height for these structures may go up to a few hundred feet. The construction of substructure for these bridges using traditional construction methodologies may not be efficient as these require the use of climbing formwork which is time-consuming and costly. Alternate solutions consist of the use of prefabricated columns but the delivery and erection of these long columns is a challenging task.

1.3 HSR Bridge Structures

In general, HSR bridges have stringent requirements for design and construction. Based on the speed, location and traveler's comfort, the structures have limitations on geometric aspect like slopes and curvatures of railway track. The track smoothness requires deflections checks which are different from conventional train bridges [Hu et al., 2014]. Besides, the bridge structures are subjected to dynamic effects of high-speed trains, fatigue and rail-deck interaction which demand bridges with higher stiffness and dynamic stability. Other structural considerations for HSR bridges include seismic performance, creep and thermal effects.

In China, the HSR lines mainly consist of standardized simply supported beams for shorter spans and continuous beams for longer spans [Hu et al.,2014]. For medium spans, Concrete Filled Tubes (CFT) arches, tied steel arch, and rigid frame prestressed structures have been used. A major portion of the Beijing-Shanghai HSR consists of simply supported prestressed box girders with a span of 32 m. Due to diverse train, long span bridges on railway network have been constructed. Most of the bridges on the German HSR network consist of simply supported bridges and continuous box girder bridges. For substructure, the most common kind of pier columns consists of reinforced concrete single columns, wall piers and, multi-column piers.

Several different design codes have been developed for HSR. China developed the Code for Design of High-Speed Railway and International Union of Railways (UIC) code provides several design leaflets for HSR. American railway engineering and maintenance-of-way association (AREMA) do not have specific requirements for high-speed rails.

The initial cost of HSR requires a large capital and due to their stringent requirements for alignment control, the construction time is an issue. For substructure construction, the use of robust construction technologies has not been used extensively for the HSR network which causes delays in delivery of the projects. To address these issues, accelerated bridge construction (ABC) technologies can assist in reducing construction time and providing solutions that are resilient and safe for construction workers. Many ABC technologies have been developed for pier construction including prefabricated piers, precast segmental and CFT columns. The use of prefabricated segmental and CFT columns have not been extensively used in HSR bridge construction.

1.4 Concrete Filled Tubes (CFT)

Concrete filled tubes (CFTs) offer an alternative to prefabricated construction which is suitable for HSRs and offer additional benefits of ABC. The use of CFTs in ABC technologies can benefit the construction industry by providing alternate structural elements which have both structural strength and ductility especially for high seismic regions such as California.

Concrete Filled Tubes (CFTs) consist of an encasing tube of steel which is filled with concrete. The tube is located at the periphery and provides protection to the in-fill concrete. The tube acts as a formwork element which reduces the cost of the structure. Most of CFTs do not require the use of any mild reinforcement inside the tube which reduces the labor cost of fabrication and assembling at the site. The structural performance of CFT is also superior to an equivalent concrete column. The steel tube offers confinement to the concrete which improves the structural capacity and ductility of the section. Under a combination of cyclic and axial load, these columns perform elastically up to a certain level of displacement after which the tubes buckle locally.

Significant research efforts have been carried out on CFT column behavior under different loading condition. Different design codes provide design expression for the CFTs including AASHTO, AISC, and ACI but the provisions of these design codes vary from each other. In building structures, CFT to steel beam connection has been extensively evaluated and used in practice (Azizinamini, 1989). However, in bridge design, there is a lack of connection design for CFT to foundation and pier cap which hinders the use of CFT especially in the U.S. Recently, there has been a lot of research effort invested in developing design recommendations on connections of CFT in bridge structures.

1.5 CFT Connection to Foundation/Cap Beam

The connection of steel tube with foundation or pier cap is to be designed to prevent any premature failure. A number of designs for CFT connection have been used in practice. The most common type of connection detail consists of exposed connection and embedded connection as shown in Figure 4. The exposed connection relies entirely on anchor bolt and thick end plate, both of which are vulnerable to damage during earthquakes. The embedded connection perform better as additional resistance is contributed by the steel tube and the concrete. However, high forces during lateral movement can cause crushing in the vicinity of the steel plate which reduces the structural performance.

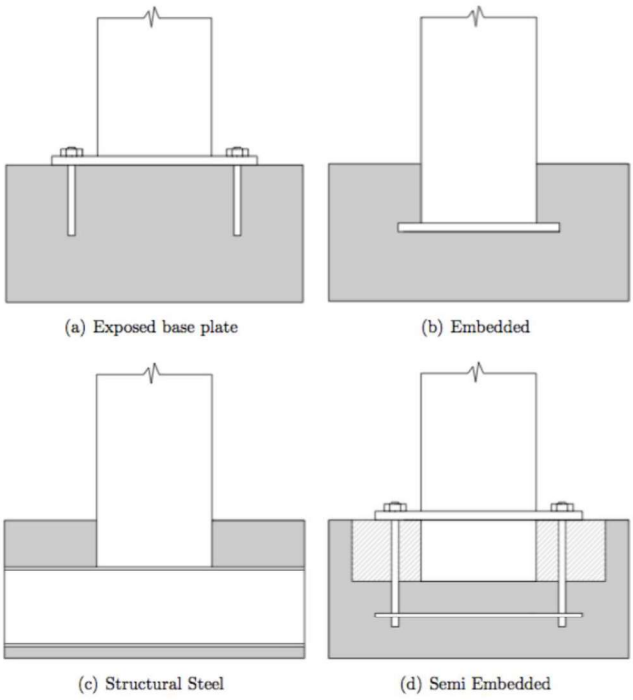

Figure 4. CFT connection a) exposed connection and b) embedded connection, c) structural steel connection, and d) semi-embedded connection (Kingsley 2005)

Hsu et al. (2006) proposed a new type of connection for square CFT by strengthening the embedded connection with stiffeners which would minimize the tendency of concrete to crush. The experimental results, under combined axial and lateral load, showed that the embedment improved the structural behavior of the connection and addition of stiffeners improved the energy dissipation capacity.

Kim et al. (2015) experimentally evaluated different types of CFT to foundation connections and compared the results on the effectiveness. Five connection details were considered with different combinations of high-tension bolts, deformed bars, and anchor frames, etc. Results showed that all columns exhibited local buckling along with anchor failures. The high-tension bolts exhibited superior structural performance when compared with anchor bolts or anchor frames.

Stephens et al. (2015) carried out an extensive experimental study on the connection of CFT column with precast concrete elements. The authors proposed different connection details (Figure 5) for foundation and cap beam which were numerically and experimentally tested and design expressions were proposed.

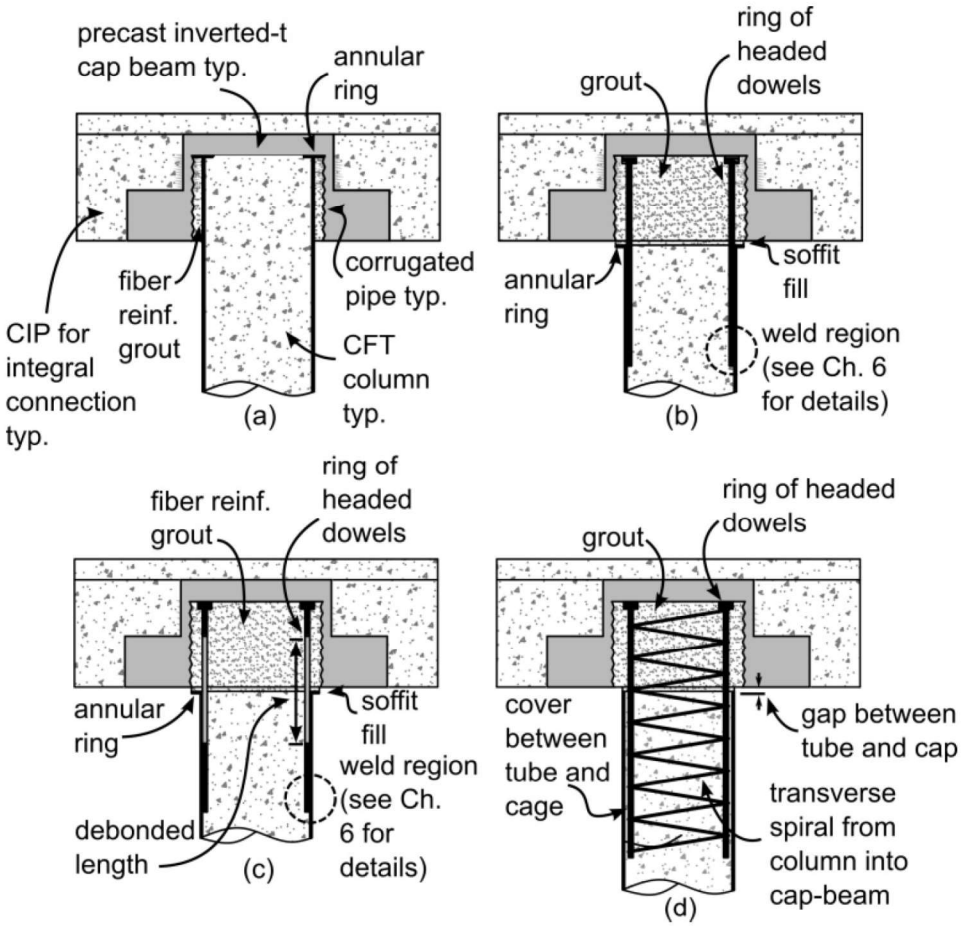

Figure 5. Proposed Connection types (Stephens, 2015)

Lehman et al. (2012) carried out an experimental study to evaluate ductile connections of CFT without the use of any dowels or internal reinforcement. The research used grouts to fill the voids once the CFT is placed in a precast member. In this case, a high-strength fiber-reinforced grout was filled to achieve composite action.

Recent research activities have looked into the use of ultra-high performance concrete (UHPC) for connecting different bridge elements. UHPC is a class of material with excellent material and durability properties. The material can exhibit compressive stress between 150-180 MPa and average tensile stress of almost 8.3 MPa. The use of UHPC for connection of precast concrete columns has been investigated by Shafieifar et al. (2018). The UHPC band at the interface of concrete column to cap beam shifted the plastic hinge away from the capacity protected element. Tazrav et al. (2015) experimentally evaluated the connection of reinforced concrete column to footing using duct connection incorporating UHPC and concluded that the connection was emulative of conventional connection. Other researchers incorporated UHPC in different configurations to protect structural elements during seismic activity. UHPC was used in plastic hinge zones of the column for pocket connections which were evaluated by Mohebbi et al. 2018.

2 Objectives and Research Approach

Previous research has demonstrated the effectiveness of an embedded and encased connection. Based on similar principles, a new concept for CFT connection is envisioned to develop the full flexural capacity of the CFT which can undergo large displacement ductility. The new connection consists of CFT embedded in the precast member and encased within a layer of UHPC. The embedment depth filled with UHPC inside the precast element provides structural strength and an encasement outside the concrete ensures that the plastic hinge is outside the footing which is typically designed as a capacity protected element. Additional dowels near UHPC layer perimeter are designed to accommodate the force transfer in the connection.

Figure 6 shows a schematic of the construction sequence. A recess, larger than the diameter of CFT, is formed in the precast reinforced concrete element with a corrugated interface. Internal and external dowels in the recess are developed in the concrete footing. Next, the CFT is placed inside the recess between the dowels.

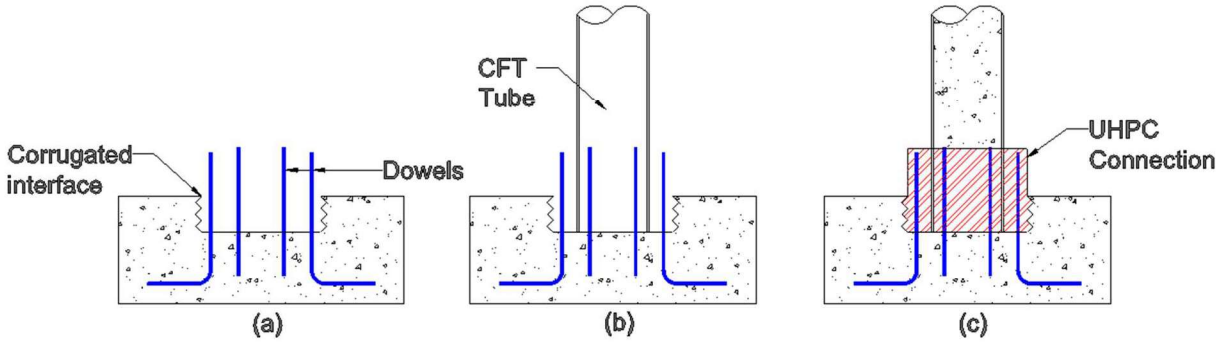

Figure 6. Proposed Connetion Detail

The recess inside the precast element and an additional outside encasement is filled with UHPC. In the final stage, the remaining CFT column is filled with NSC. To resist slippage and improve the transfer of forces from CFT to UHPC, different details can be used such as the inclusion of shear connectors, threaded rods, ring plates or a combination of these. The embedded layer is designed for pullout resistance and the precast concrete is checked for punching shear. The depth of the UHPC layer is controlled by the anchorage requirements of the dowels. On the other hand, the diameter of the UHPC layer should be adequate to provide a cover of at least three times dowel diameter ($3d_b$) for perimeter dowels. The sequence of construction is suitable for ABC applications for construction of footings and cap beams. Different details are envisioned for the connection of CFT-to-footing. Among the possible options, three main parameters are investigated. This includes a) the location of UHPC layer (embedded vs enchased vs partially enchased), b) the type of transfer mechanism (shear connecters, threaded rods, ring plates), and 3) embedment depth.

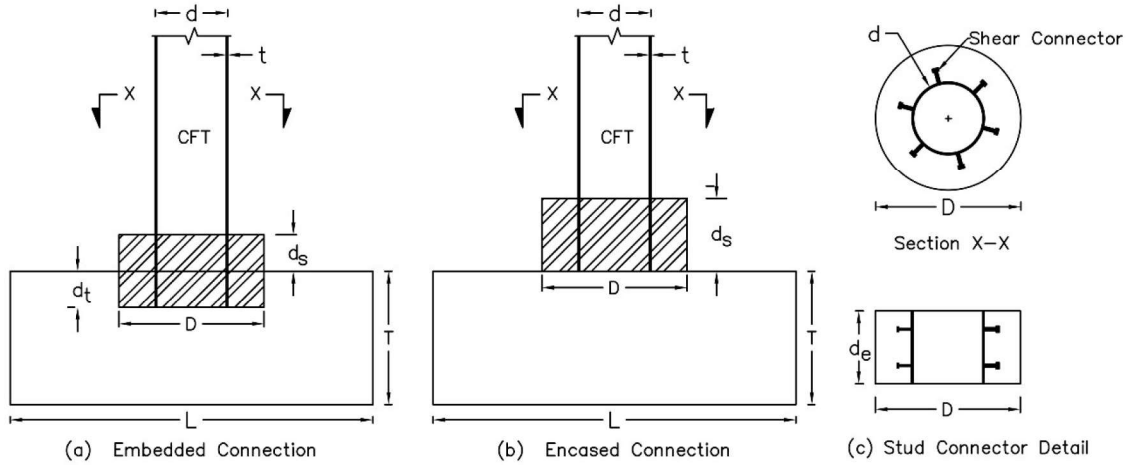

Figure 7. Connection parameters

The development of dowels and the width of the UHPC layer is dependent on the minimum embedment depth of the reinforcing dowels and the cover requirements. Figure 7 shows the schematic and geometric variables of the specimen. The embedment depth is comprised of two components, d_t (depth of embedment in footing) and d_s (depth of encasement), which are encased in a layer of UHPC, d_t (UHPC depth) which is sum of both d_t and d_s. The width (D) of the UHPC layer depends on the outside diameter (d) of the CFT and additional width required to encase dowels within cover requirements of UHPC. The geometrical variables of the precast footing including length (L) and thickness (T) which are also shown in Figure 7. Based on these different options discussed above, a possible test specimen matrix is developed in Table 1.

Table 1 Possible matrix of test specimen

Specimen No.	Connection type	Shear Connector (No.)	UHPC Depth (d_e)	UHPC layer Diameter (D)
1	Partially Embedded	18	1.0 d	24 in
2	Encased	18	0.85 d	24 in

3 Experimental Study

Based on the envisioned connection, an experimental program is established at Florida International University (FIU). In the first series of testing, two connections are being tested i) a partially embedded connection with UHPC encasement and ii) an encased connection. The material and geometric properties of different sections are used to calculate the capacity of the section for the test specimen (Table 2). The CFT column consists of spiral weld tube which conforms to ASTM A252 standards. The compressive strength of NSC and UHPC were assumed to be 6.5 ksi and 24 ksi, respectively. For the test specimen, the outer diameter of the CFT column is 12.75-in with a wall thickness of 0.25-in. The shear connectors consist of 0.75-in diameter deformed reinforcing steel which conforms to the ASTM A615 specification. The shear connectors used in the specimen had a shaft diameter of 0.5-in, and an aspect ratio of 5.

Table 2 Design Parameters and Material Properties of Specimen 1 & Specimen 2

Parameters	Specimen -1	Specimen -2
Diameter to thickness ratio (*d/t*)	51	51
Axial capacity (P_o)	1310 kips	1310 kips
Axial load ratio	10 %	10 %
Length of column to diameter ratio (*l/d*)	5.1	4.6
Embedded depth (d_t)	0.5 d	-
Encased depth (d_s)	0.5 d	0.85 d
UHPC layer depth (d_e)	1.0 d	0.85 d
Steel tube yield (f_{yt})	45 ksi	45 ksi
UHPC compressive strength (f'_{uhpc})	24 ksi	24 ksi
NSC compressive strength (f'_c)	6.5 ksi	6.5 ksi
Expected yield strength of reinforcing bars (f_y)	470 ksi	68 ksi

3.1 Design of Test Specimen-1

Specimen-1 was designed as an embedded connection which consists of a total of 18 shear connectors that are welded to the tube made of low carbon steel conforming to ASTM A29. The clear cover thickness over the head of the shear connector was 5-in which conforms to the AASHTO-LRFD specification (AASHTO, 2012). The diameter-to-depth (d/t) ratio of the CFT column was 51 which is less than 87 based on AISC specifications (AISC). This limit ensures the local stability of the tube. The UHPC layer depth ($d_e=d_t+d_s$) is taken as 1.0 x internal diameter of the column (d). The recess in the specimen is octagonally shaped with a maximum dimension of 24-in. This recess was corrugated to provide a composite action with the adjacent NSC. Based on Caltrans provisions, the connection is designed to resist the maximum over-strength moment which is defined as 1.2 times the plastic moment capacity of the column. For specimen-1 design, the capacity is evaluated at different sections such as CFT section (A-A), UHPC layer section (B-B), and footing section (C-C). Moment-curvature analyses were conducted for sections at these locations using fiber approach, and the moment capacities of the sections are provided in Table 3. Based on over-strength requirements, the concrete section was proportioned, and the reinforcement was determined as shown in Figure 8.

Table 3 Moment capacity of the section (specimen-1)

Specimen No.	Moment (M_1) at Sec A-A	Moment (M_2) at Sec B-B	Moment (M_3) at Sec C-C	M_1/M_2	M_3/M_2
Specimen 1	815 Kip-ft	228 Kip-ft	356 Kip-ft	4.85	2.1

Figure 9 shows the sequence of construction for specimen-1. In the first stage, a prefabricated footing was cast with a recess. The recess was fabricated into the footing using Styrofoam mold. The profile of the Styrofoam was corrugated at its circumference to allow transfer of forces between UHPC and adjacent concrete footing. Before casting, the mold was embedded in the footing and NSC was cast. After the curing, the Styrofoam mold was removed and the interface at the bottom surface of the recess was chipped off to improve bond between the footing concrete and the UHPC. To allow UHPC to flow inside the CFT, two grooves were cut at the bottom of the CFT. In the encasement region, a total of 18 shear connectors were welded (using

arc welding method) equidistant around the tube. An encasement formwork was placed with a 12-in Sonotube and the CFT tube was placed inside the recess. Then the UHPC was cast into the recess for a total depth of 12-in with 6-in encasement above the footing. A concrete loading block is constructed at the top to apply incremental lateral cyclic and constant axial load.

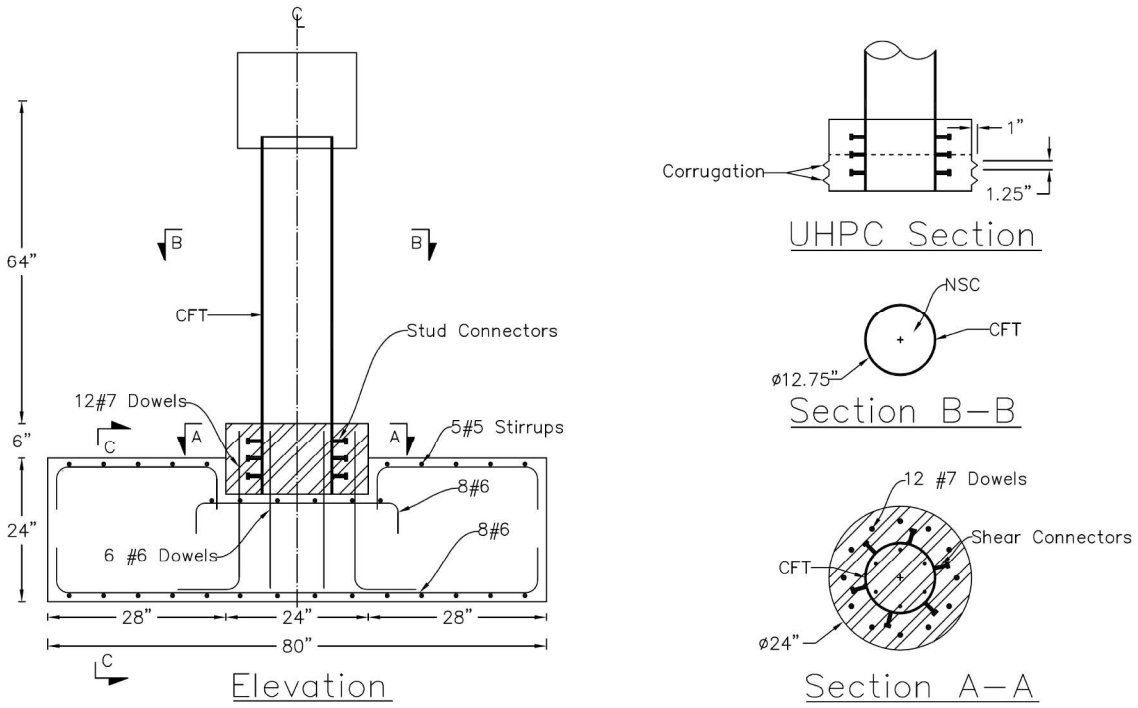

Figure 8: Reinforcement detail Specimen-1

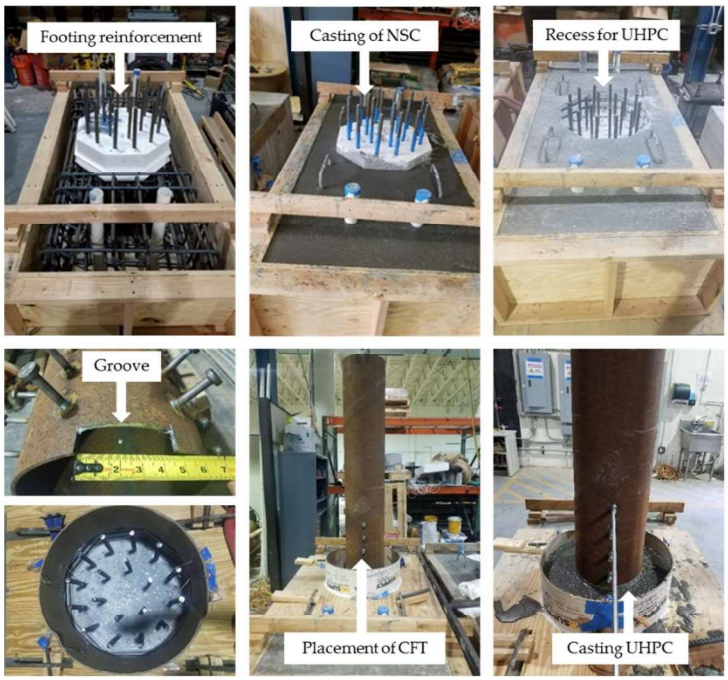

Figure 9. Construction of Specimen-1

3.2 Design of Test Specimen -2

The specimen-2 was an encased type connection which consists of a total of 18 shear connectors to transfer forces at the connection. The embedment length (d_s) was taken as 0.85 x internal diameter of the column (d). No recess was required in this type of connection which translates into simpler reinforcement details for the footing. The encasement in the specimen is 24-in diameter. The interface between the footing concrete and UHPC encasement is roughened to improve the bond at the interface. Similar to specimen-1, the capacities of sections are evaluated at different sections such as CFT section (A-A), UHPC layer section (B-B), and footing section (C-C). Moment-curvature analyses were conducted for sections at these locations using fiber approach, and the moment capacities of the sections are provided in Table 4. Based on over-strength requirements, the concrete section is proportioned, and the reinforcement is determined as shown in Figure 10.

Table 4 Moment capacity of the section (specimen-2)

Specimen No.	Moment (M_1) at Sec A-A	Moment (M_2) at Sec B-B	Moment (M_3) at Sec C-C	M_1/M_2	M_3/M_2
Specimen 2	975 K-ft	228 k-ft	535 k-ft	4.2	2.4

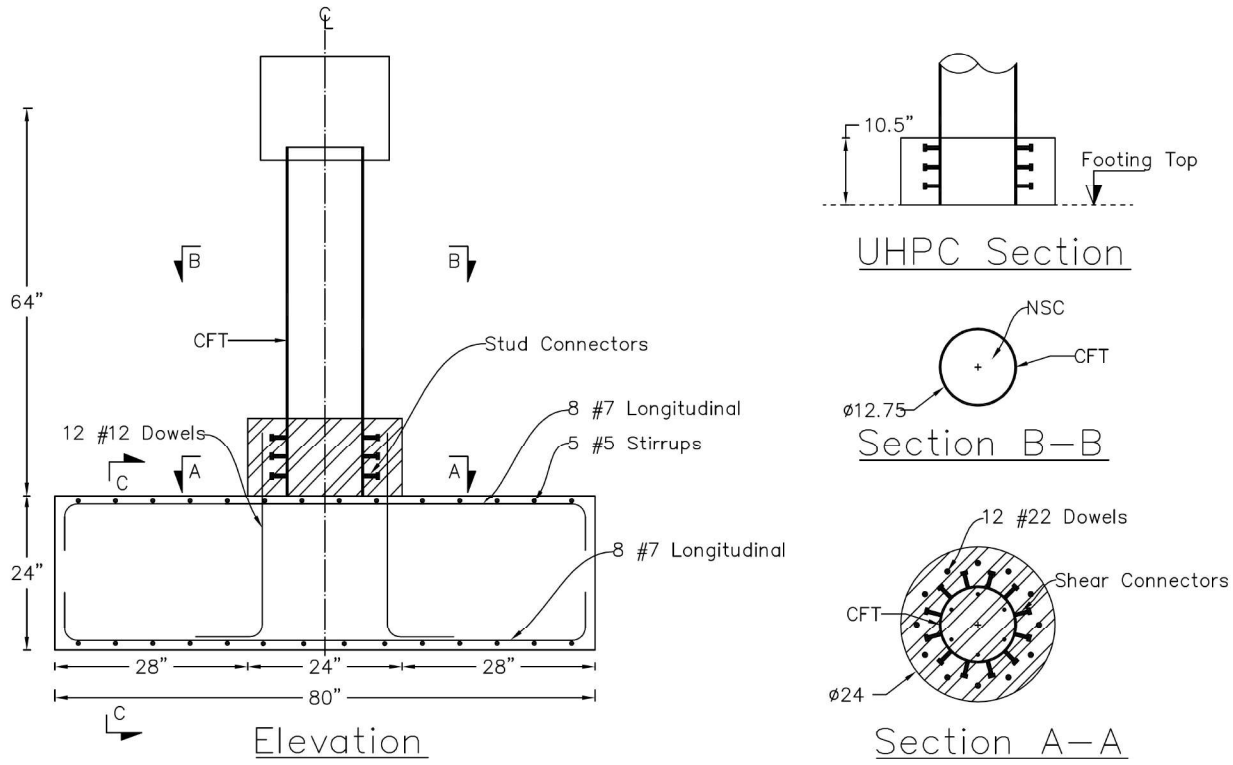

Figure 10. Reinforcement detail of Specimen-2

The footing reinforcing bars with dowels were placed before casting of normal concrete. Figure 11 shows pictures of the construction sequence described above. After casting of normal concrete of footing, the interface between UHPC encasement and the footing was roughened to

about half-inch depth. The dowel bars and the steel tube were instrumented with strain gages prior to the casting of UHPC. The encasement layer was cast using a sonotube of 24-inch diameter and a depth of 10 inches. Like specimen-1, two grooves were cut at the bottom of the CFT to allow UHPC to flow inside the tube. After casting of UHPC encasement, the steel tube was filled with normal concrete. A concrete cap was also cast at the same time which is reacted against the hydraulic ram. The specimen-2 is currently under testing phase. The results for this specimen will be reported in the next reporting.

Figure 11. Construction of Specimen-2

3.3 Test Setup and Testing Protocol

The specimen was designed to be tested in a cantilever configuration. The cyclic load is applied on loading block using a 150-kips servo-hydraulic actuator. The cyclic load is based on displacement-control loading scheme which is applied as incremental drift ratios. Based on the assumed material properties of the CFT, the pure axial capacity of the column is about 1310 kips. For the axial load, 10% of pure axial load capacity, is to be applied on the top of the specimen through a spreader beam using hydraulic jacks. Prior to testing, the specimen is instrumented extensively with string potentiometers, steel strain gauges, linear potentiometers, and load cells which are tabulated in Table 5. The test setup and some of the instruments are shown in Figure 12. The dowels were typically instrumented with strain gauges at critical locations. Two strain gages were located inside the concrete footing and one was located in the UHPC encasement for four dowels. Similarly, strain gauges were also installed on the outer surface of the CFT tube at different depths. Coupling nuts were also welded on the steel tube to allow for the installation of linear potentiometers. Video cameras were used to record the damage of the specimen throughout the test.

The response of the test specimen during the test is typically monitored to evaluate the connection under a combination of cyclic and axial loadings. Displacement-control cyclic loads with increments of first yield displacement, Δ_y, are to be applied to the CFT until failure. The first yield displacement of the column can be estimated during the first cycles from idealized bi-linear models. Observations for damages and failure mode are typically performed at different displacement levels.

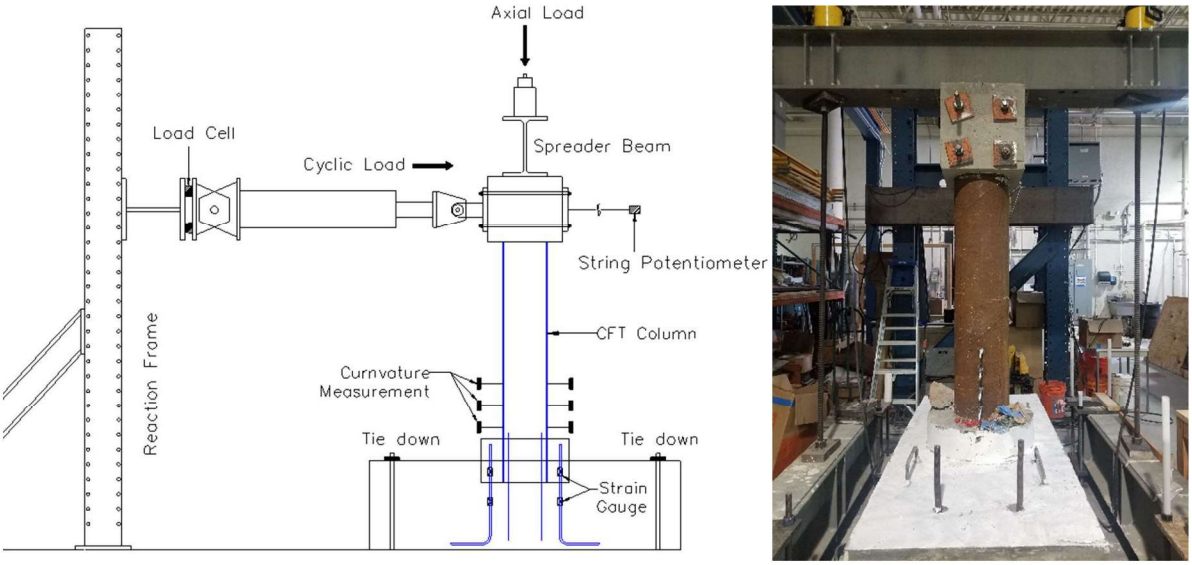

Figure 12. Load test setup

Table 5 Instrumentation Summary

Parameters	Description
Load Cells	3
Steel dowel strain gauges	13
Steel tube strain gauges	21
String Potentiometer	2
Linear Potentiometers	8
Pressure Transducers	2

3.4 Experimental Results

3.4.1 Specimen-1

The response of the test specimen-1 during the test was monitored to evaluate the connection under a combination of cyclic and axial loadings. Displacement-control cyclic loads with increments of first yield displacement, Δ_y, were applied to the CFT until failure. The first yield displacement of the column was estimated during the first cycles from idealized bi-linear models. Observations for damages and failure mode were typically performed at different displacement levels. During the initial cycles, there were minimal cracking in the UHPC encasement. This cracking is attributed to a construction shortcoming from a void was left during casting. However, no major cracking was observed after initial cycles.

Figure 13. Ductile tearing of the CFT (left), and crack pattern in UHPC step (right)

As shown in Figure 13, the tube failed through ductile tearing during the second cycle of $7\Delta_y$. The system showed a composite behavior at the encasement location and minimal separation between the tube and the surrounding UHPC. The ductile tearing of the CFT is a desired mode of failure while the capacity protected (footing) element remained elastic.

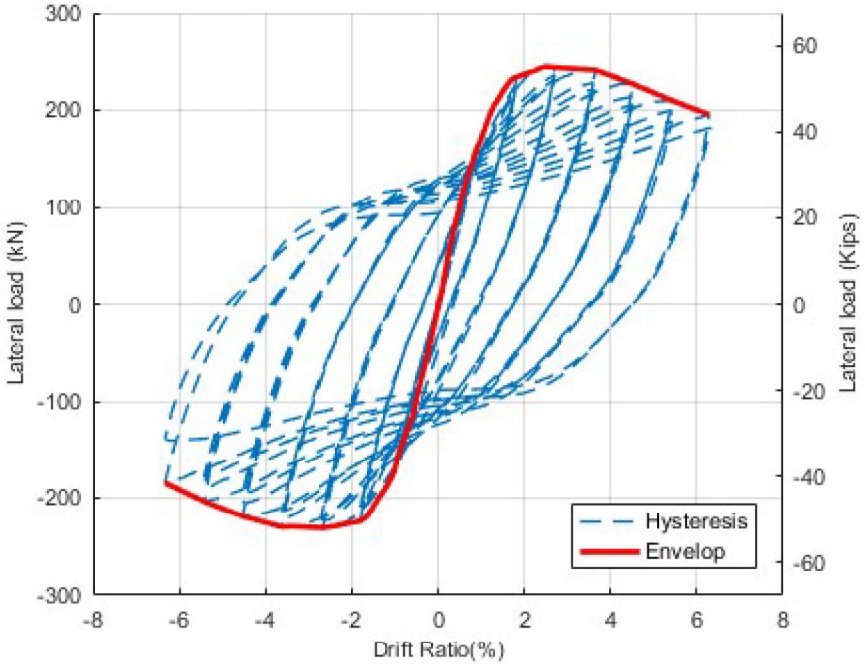

Figure 14. Load vs Drift ratio

Strains were observed for the dowel bars and footing longitudinal reinforcing bars and results showed that these reinforcing bars did not reach their yield point. As shown in Figure 14, the force displacement hysteresis curve showed a symmetrical response with sufficient ductility and energy dissipation. The column was able to reach a drift ratio of about 6.3. Strains in tube were measured at different heights above the concrete footing which are shown in Figure 15 (left). It can be observed that the critical section was located above the UHPC encasement while the strain gages located inside the footing either remained below or about the yield point.

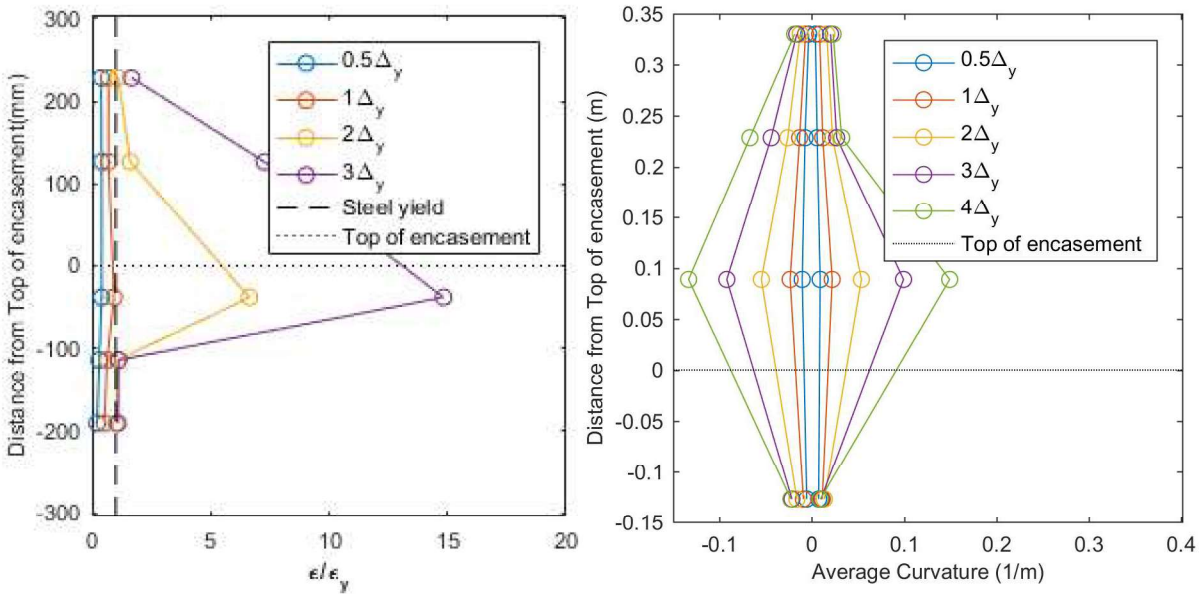

Figure 15. Steel tube strains near UHPC step (left) and curvatures at different Δ_y

The data at higher drift ratios are not reported since the strain gages were damaged at these levels. Curvature was also measured at the encasement level and results are plotted in Figure 15 (right). Average curvatures are reported at these heights since buckling of the tube caused inconsistencies in measurement system.

3.4.2 Specimen-2

Similar to Specimen-1, Specimen-2 was also subjected to a combination of lateral cyclic and constant axial load. Displacement-control cyclic loads with increments of first yield displacement, Δ_y, were applied to the specimen until failure. The first yield displacement of the column was estimated during the first cycle from idealized bi-linear models. During testing, observations were made for damages and failure mode. At the initial displacement level, cracks were observed in the UHPC encasement. These cracks increased with an increase in displacement levels. Also, the top layer of shear connectors protruded out of the top layer of encasement. This failure of the first layer of shear connectors resulted in a decrease in the lateral load-carrying capacity. The crack pattern and failure in UHPC encasement is shown are Figure 16. The testing was continued up to $7\Delta_y$ with a progressive increase of cracking in the vicinity of the shear connectors. However, the specimen was able to sustain further load as the other two layers of shear connectors were engaged. The footing did not sustain any damage during the testing.

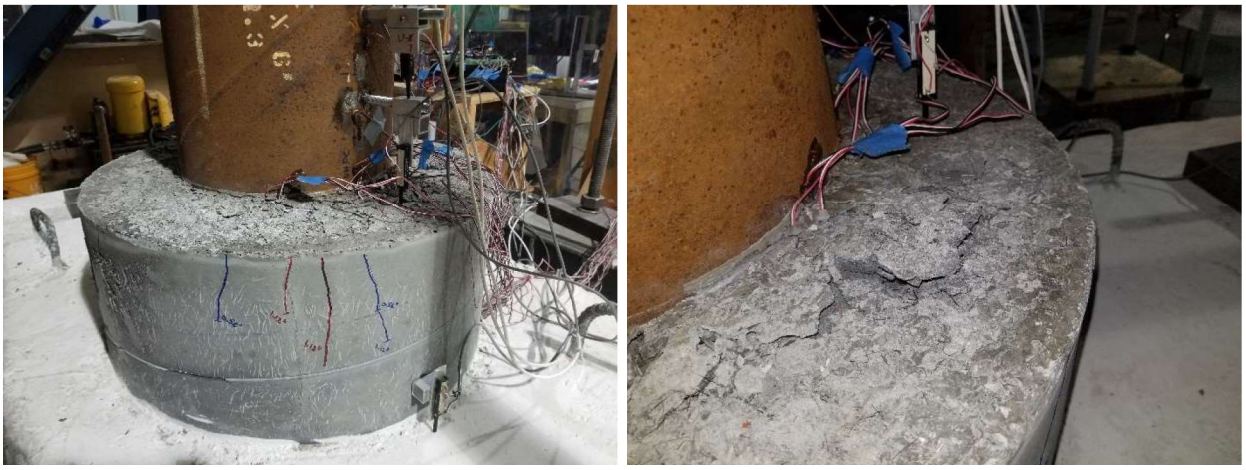

Figure 16. Crack pattern in UHPC encasement

The CFT column did not fail until $7\Delta_y$ and testing was terminated due to limitation of the test setup. The lateral load vs drift ratio is plotted in Figure 17. The specimen exhibited smaller areas of hysteresis loops if compared to Specimen-1, implying a lower energy dissipation capacity. The abrupt change in the plot occurred due to opening and closing of the cracks near the first layer of shear connectors.

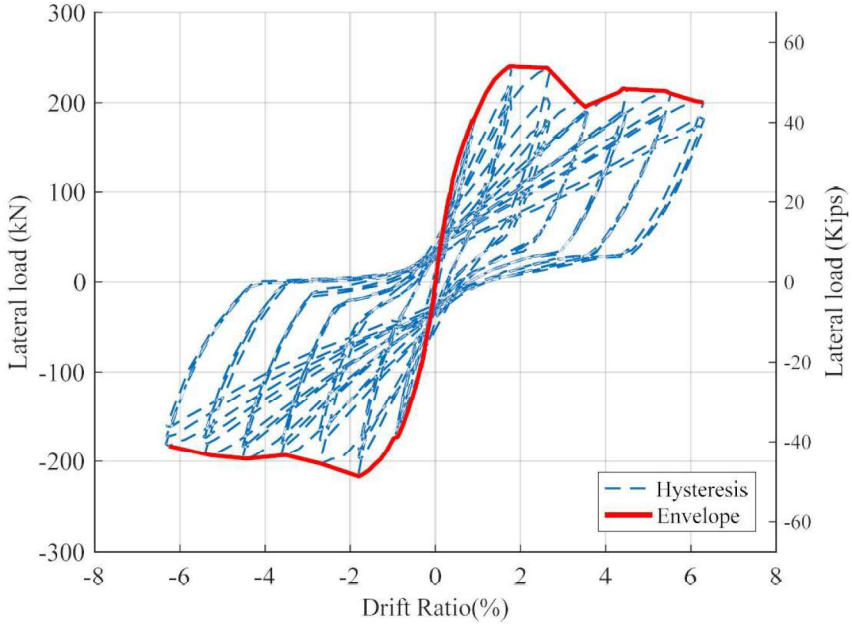

Figure 17. Load vs Drift Ratio

Strains were observed along the bottom part of the steel tube for both north and south ends. As shown in Figure 18, It can be observed that the critical section was located at the termination of UHPC encasement and the strain exceeded the yield point of the steel tube.

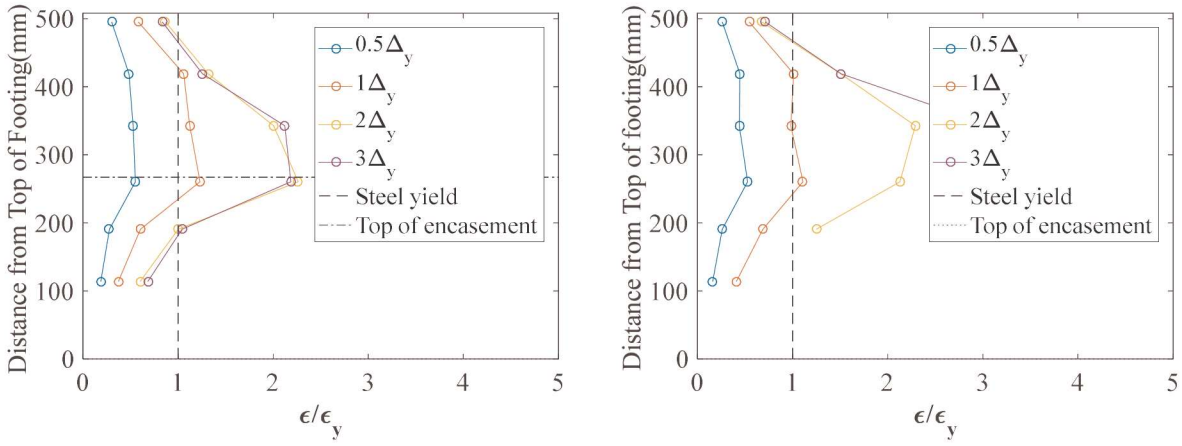

Figure 18. Steel tube strains at North (left) and South (right) end of steel tube

4 Discussion and Preliminary Conclusions

This research presented a new detail for CFT connections to precast members using a UHPC layer which is proposed for ABC application. A literature review of past research has shown the effectiveness of embedded and encased connection over other CFT connections such as steel base plate connections. Due to high mechanical strength of UHPC, the embedment can be reduced compared to grouted or NSC layer. An analytical study was performed to evaluate the specimen flexural capacity at critical sections. Based on this analysis, an experiment is designed to evaluate the performance under a combination of constant axial and incremental lateral cyclic loads. The results of specimen-1 showed that the CFT underwent ductile tearing of the tube which was the preferred mode of failure while the footing is designed as capacity protected element did not undergo any damage. The specimen-2 failed due to shear connectors puncturing out from the top of the UHPC encasement. The specimen exhibited lower energy dissipation capacity and extensive cracking was observed in the UHPC layer.

To complement the experimental study, a finite element analysis is planned to be carried out. The calibrated finite element model will be used to perform a parametric study on the effect of 1) embedment depth, 2) encasement diameter and depth and 3) the anchorage provided by shear connectors to extend the experimental program.

5 Schedule

Progress of tasks in this project are shown in the table below.

Item	% Completed
Percentage of Completion of this project to Date	90%

Phase	Research Task	Jan 2019 – Dec 2019						Jan 2020 – June 2020					
1	Task 1 – Literature Review												
	Task 2 – Review of Design Provisions for HSR												
	Task 3 – Envisioning connection details												
	Task 4 – Proof of Concept Experimental Work												
	Task 5 – Final Report												
				Work Performed									
				Works to be Performed									

6 References:

1. Azizinamini, A., & Radziminski, J. B. (1989). Static and cyclic performance of semirigid steel beam-to-column connections. *Journal of Structural Engineering*, *115*(12), 2979-2999.
2. Campos, J., & De Rus, G. (2009). Some stylized facts about high-speed rail: A review of HSR experiences around the world. *Transport policy*, *16*(1), 19-28.
3. Dobruszkes, F. (2011). High-speed rail and air transport competition in Western Europe: A supply-oriented perspective. *Transport policy*, *18*(6), 870-879.
4. Gourvish, T. (2010). The high speed rail revolution: history and prospects. *London: HS2 Ltd*.
5. Hsu, H. L., & Lin, H. W. (2006). Improving seismic performance of concrete-filled tube to base connections. Journal of Constructional Steel Research, 62(12), 1333-1340.
6. Hu, N., Dai, G. L., Yan, B., & Liu, K. (2014). Recent development of design and construction of medium and long span high-speed railway bridges in China. Engineering Structures, 74, 233-241.
7. Kang, C., Schneider, S., Wenner, M., & Marx, S. (2018). Development of design and construction of high-speed railway bridges in Germany. Engineering Structures, 163, 184-196.
8. Kim, H. J., Hu, J. W., & Hwang, W. S. (2015). Cyclic testing for structural detail improvement of CFT column-foundation connections. Sustainability, 7(5), 5260-5281.
9. Kingsley, A. M. (2005). Experimental and analytical investigation of embedded column base connections for concrete filled high strength steel tubes (Doctoral dissertation, University of Washington).
10. Lehman, D. E., & Roeder, C. W. (2012). Foundation connections for circular concrete-filled tubes. Journal of Constructional Steel Research, 78, 212-225.
11. Mohebbi, A., Saiidi, M. S., & Itani, A. M. (2018). Shake Table Studies and Analysis of a PT-UHPC Bridge Column with Pocket Connection. Journal of Structural Engineering, 144(4), 04018021.
12. Qin, S., & Gao, Z. (2017). Developments and prospects of long-span high-speed railway bridge technologies in China. Engineering, 3(6), 787-794.

13. Shafieifar, M., Farzad, M., & Azizinamini, A. (2018). New Connection Detail to Connect Precast Column to Cap Beam using Ultra-High-Performance Concrete in Accelerated Bridge Construction Applications. Transportation Research Record, 0361198118792766.
14. Stephens, M. T., Lehman, D. E., & Roeder, C. W. (2015). Concrete-filled tube bridge pier connections for accelerated bridge construction (No. CA15-2417).
15. Tazarv, M., & Saiidi, M. S. (2015). UHPC-filled duct connections for accelerated bridge construction of RC columns in high seismic zones. Engineering Structures, 99, 413-422.
16. AISC 360-16. American Institute of Steel Construction 360-16: Specification for Structural Steel Buildings. 2016.
17. AASHTO. LRFD Bridge Design Specifications. Washington, D.C., 2012.